INTERNATIONAL JOURNAL OF HYDROGEN ENERGY 42 (2017) 4051–4060

Available online at www.sciencedirect.com

ScienceDirect

journal homepage: www.elsevier.com/locate/he

Production of bio-hydrogen by liquid processing of xylitol on Pt/Al_2O_3 catalysts: Effect of the metal loading

H.A. Duarte, M.E. Sad, C.R. Apesteguía *

Catalysis Science and Engineering Research Group (GICIC), INCAPE, UNL-CONICET, Predio CCT Conicet, Paraje El Pozo, 3000 Santa Fe, Argentina

ARTICLE INFO

Article history:
Received 22 August 2016
Received in revised form
26 October 2016
Accepted 16 November 2016
Available online 8 December 2016

Keywords:
Bio-hydrogen
Aqueous-phase reforming
Xylitol
H_2 production
Pt/Al_2O_3 catalysts
Green chemistry

ABSTRACT

The aqueous-phase reforming of xylitol to produce bio-hydrogen was studied on Pt/Al_2O_3 catalysts containing 0.30, 0.57, 1.50 and 2.77%wt Pt by varying the weight hourly space velocity (WHSV) between 0.6 and 2.4 h^{-1}. At a constant WHSV value, the gaseous/liquid products ratio depended on the amount of surface Pt concentration on the sample (Pt_s). The xylitol conversion to gaseous products increased with Pt_s while xylitol conversion to liquid products did not change significantly. At a constant xylitol conversion, the H_2 selectivity increased with Pt_s. The H_2 yield increased continuously with both contact time and Pt_s. The H_2 productivity (Pr, mmol H_2/h g_{cat}) increased with both WHSV and Pt_s; indeed, the maximum Pr value obtained when using 1% xylitol in the feed (28 mmol H_2/g_{cat} h) was obtained on $Pt(2.77)/Al_2O_3$ catalysts at WHSV = 2.4 h^{-1}. The effect of the xylitol concentration on H_2 productivity was also investigated. At a constant space velocity, the H_2 selectivity and productivity decreased with increasing xylitol concentration in the feed.

Introduction

The production of bio-hydrogen via biomass-derived compounds is currently a subject of industrial and economical importance because hydrogen is not only an alternative energy source but also one of the key reactants to produce chemicals from conversion of natural renewable resources [1,2]. Although the high-water content of biomass turns it unsuitable for steam reforming processes, the liquid-phase reforming of biomass appears as a promising technology to produce bio-hydrogen. Pioneering work in aqueous-phase reforming (APR) with specific aim of hydrogen production from polyols was carried out by Dumesic and co-workers [3]. The APR process allows to generate hydrogen in a single reactor at low temperatures (473–543 K), compared with conventional reforming, which favors the water-gas shift reaction producing only traces of carbon monoxide. Operation at low temperatures also reduces energy costs of water vaporization and allows processing feedstocks sensitive to thermal decomposition. The APR of polyols to produce hydrogen was initially studied using shorter substrates such as ethylene glycol and glycerol [4–8]. Then, several papers have investigated the APR of larger substrates such as glucose

* *Corresponding author*. INCAPE, Predio CCT Conicet, Paraje El Pozo, 3000 Santa Fe, Argentina.
E-mail address: capesteg@fiq.unl.edu.ar (C.R. Apesteguía).
URL: http://www.fiq.unl.edu.ar/gicic

http://dx.doi.org/10.1016/j.ijhydene.2016.11.119

[9,10] and sorbitol [11–15], a sugar alcohol obtained by hydrogenation of glucose. Recently, the APR of xylitol, a five-carbon sugar alcohol derived from xylose hydrogenation, has been studied [16–20]. Although the H_2 yield diminishes with the reactant size [3,21], the liquid processing of larger substrates is economical attractive because minimizes pretreatment costs.

The reaction pathway to produce hydrogen by APR of biomass-derived oxygenated hydrocarbons involves the cleavage of C–C, C–H and O–H bonds on metal sites forming adsorbed CO that consecutively reacts with water to yield H_2 and CO_2 via the forward water–gas shift (WGS) reaction. This reaction pathway is depicted in Fig. 1 for the conversion of xylitol and shows the initial reactant decarbonylation (reaction 1) followed by the WGS reaction (reaction 2) that account for the stoichiometry of H_2 and CO_2 formed (reaction 3):

$$C_5O_5H_{12} \rightarrow 5\ CO + 6\ H_2 \quad (1)$$

$$5\ CO + 5\ H_2O \rightarrow 5\ CO_2 + 5\ H_2 \quad (2)$$

$$C_5O_5H_{12} + 5\ H_2O \rightarrow 5\ CO_2 + 11\ H_2 \quad (3)$$

Nevertheless, the selective formation of H_2 via APR of polyols is challenged by undesired parallel/consecutive reactions proceeding via cleavage of C–O bonds that form liquid alkanes and oxygenates [22]. The development of highly active catalysts that selectively promote the desired reaction pathways is then required to obtain competing technologies for generating hydrogen from liquid processing of polyols.

Few studies have been published addressing the selective production of H_2 from APR of xylitol [15,17–19]. Xylitol is obtained by catalytic hydrogenation of xylose monomer which is the major building block for the hemicellulose xylan, one of the main constituents of wood [23]. The content of xylose in the xylan-rich portion of hemicellulose, present in plant cell walls and fiber, can reach 25–30% in some species of hardwood [24,25]. Thus, xylitol is the second most abundant polyol resulting from lignocellulosic industry and provides a potential route for the sustainable production of hydrogen from natural renewable resources. Among the catalysts employed in these papers (monometallic Pt-supported on carbon, TiO_2, and Al_2O_3 and bimetallic Pt–Re/TiO_2) Pt/Al_2O_3 showed superior performance regarding hydrogen productivity. Actually, the literature shows that Pt/Al_2O_3 catalysts have been widely employed for the APR of polyols, probably because Pt is more selective for H_2 production than other noble metals [26] and alumina does not contain strong surface acid sites for promoting the acid catalyzed dehydration of xylitol [27]. The development of competing technology for generating hydrogen from biomass requires the use of highly active, selective and cost-effective catalysts for achieving optimal H_2 productivity that is the key parameter to evaluate the economic feasibility of using bio-hydrogen as an energy vector. Due to the high cost and limited availability of Pt, it is significant to establish what is the Pt loading required to obtain active, selective and stable catalysts for achieving the highest H_2 productivity. The effect of Pt particle size on the activity of Pt-supported catalysts has been investigated for the aqueous-phase reforming of glycerol [6,28] and ethylene glycol [29]. However, no studies have been performed on the effect of Pt surface concentration on both the gaseous/liquid products ratio and the H_2 productivity for liquid processing of xylitol. Precisely, we investigate here the APR of xylitol on Pt/Al_2O_3 catalysts containing different amounts of platinum, between 0.30% and 2.77% Pt. Results show that the hydrogen productivity obtained by liquid processing of xylitol may be regulated by the platinum surface concentration on the catalyst. At a given space velocity, the H_2 productivity increases continuously with the Pt surface concentration but reaches a plateau at about 40 μmol Pt/g that in our case corresponded to a Pt/Al_2O_3 catalysts containing 1.50% Pt.

Experimental

Catalyst preparation and characterization

Pt/Al_2O_3 catalysts with 0.30, 0.57, 1.50 and 2.77%wt Pt were prepared by incipient wetness impregnation. A high-purity γ-Al_2O_3 powder (Cyanamid Ketjen CK300) of 220 m^2/g BET specific surface area and 0.49 cm^3/g pore volume was impregnated at 303 K with a solution of tetraamine platinum nitrate, $Pt(NH_3)_4(NO_3)_2$ (Aldrich, 99.99%). After impregnation,

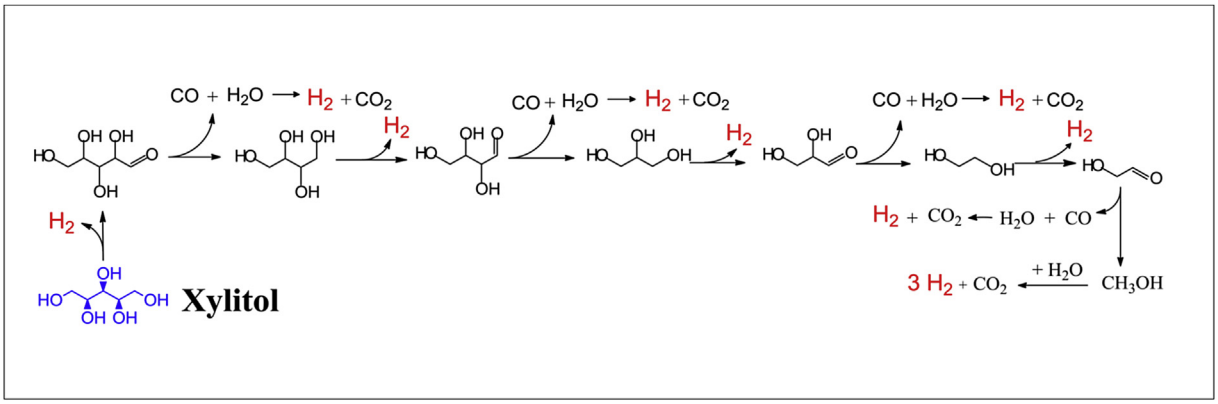

Fig. 1 – Scheme of the production of H_2 by the APR of xylitol.

the samples were dried 12 h at 353 K, heated in air at 773 K for 3 h and finally reduced 2 h at 773 K in pure hydrogen.

Total surface areas (S_{BET}, m^2/g) were measured by N_2 physisorption at its boiling point using a Autosorb Quantochrome Instrument 1-C sorptometer and BET analysis methods. Prior to N_2 physisorption, the samples were outgassed for 1 h at 623 K. Pt loadings were measured by inductively coupled plasma atomic emission spectroscopy (ICP-AES), using a Perkin–Elmer Optima 2100 unit. The Pt dispersion (D_{Pt}, surface Pt atoms/total Pt atoms) of the samples was determined by hydrogen chemisorption. The volumetric adsorption experiments were performed at room temperature in a conventional vacuum apparatus. Hydrogen uptake was determined using the double isotherm method: the first isotherm gave the total gas uptake and the second, obtained after 1 h of evacuation at room temperature, the weakly adsorbed gas. By difference, the amount of strongly adsorbed gas was determined. The pressure range was 0–7 kPa and extrapolation to zero pressure was used as a measure of the gas uptake on the metal. Samples were reduced in H_2 at 673 K and then outgassed 2 h at 673 K for 2 h prior to performing gas chemisorption experiments. A stoichiometric atomic ratio of $H/Pt_s = 1$, where Pt_s implies a Pt atom on surface, was used to calculate the Pt dispersion. Mean Pt crystallite sizes ($\bar{d}_{Pt}$, nm) were determined from H_2 chemisorption data by using site densities of 1.12×10^{15} sites per cm^2 of metal [30].

Fresh and used Pt/Al_2O_3 catalysts were analyzed by transmission electron microscopy (TEM) using a JEOL 100 CX II microscope with an acceleration voltage of 100 KV and magnification of 450,000×. A significant number of Pt particles were observed to obtain reliable particle size distribution histograms. The average volume/area diameter of Pt crystallites (d_{VA}, nm) was calculated from: $d_{VA} = \frac{\sum n_i d_i^3}{\sum n_i d_i^2}$, where n_i is the number of Pt particles of size d_i.

The solid structure of Al_2O_3 and Pt/Al_2O_3 samples were determined by powder X-ray diffraction (XRD) methods using a Shimadzu XD-D1 diffractometer and Ni-filtered CuKα radiation. Acid site densities were determined by using temperature-programmed desorption (TPD) of NH_3 preadsorbed at 373 K. Samples (200 mg) were treated in He (60 cm^3/min) at 773 K for 1.5 h and then exposed to a 1% NH_3/He stream for 40 min at 373 K. Weakly adsorbed NH_3 was removed by flushing with He at 373 K for 0.5 h. Temperature was then increased at 10 K/min and the NH_3 concentration in the effluent was measured by mass spectrometry (MS) in a Baltzers Omnistar unit.

The nature of surface acid sites on alumina was determined by Fourier infrared transform spectroscopy (FTIR) of adsorbed pyridine using a Shimadzu FTIR-8101 M spectrophotometer. Samples were ground to a fine powder and pressed into wafers (20–40 mg). The discs were mounted in a quartz sample holder and transferred to an inverted T-shaped Pyrex cell equipped with CaF_2 windows. Samples were initially outgassed in vacuum at 723 K during 2 h and then a background spectrum was recorded after being cooled down to room temperature. Spectra were recorded at room temperature, after admission of pyridine, and sequential evacuation at 303 and 373 K.

Catalytic testing

All the samples were tested for the APR of xylitol in a plug-flow packed-bed reactor at 498 K and 29.3 bar using aqueous solutions containing 1–10%wt xylitol (Sigma Aldrich, 99.9%). Catalysts (0.35–0.42 mm) were reduced in-situ at 573 K with pure H_2 (75 cm^3/min) for 1 h before reaction. The feed was introduced to the reactor in a N_2 carrier flow using a HPLC-type pump (Alltech 310) and pressurized to setpoint. The reactor effluent was cooled down by passing through a condensation system and then conducted to a gas–liquid separator. A Shimadzu GC-2014 gas chromatograph equipped with a Hayesep D 100–120 column (5 m × 1/8 in × 2.1 mm), and thermal conductivity (TCD) and flame ionization (FID) detectors was used to analyze on line the gaseous products. Hydrogen was quantified using the TCD detector while CO, CO_2 and CH_4 were analyzed by FID after completely converting CO and CO_2 to methane by means of a methanation catalyst (Ni/Kieselguhr) operating at 673 K. Condensable products were drained periodically and quantified by using high-performance liquid chromatography (HPLC) in a UFLC Shimadzu Prominence chromatograph equipped with a BioRad Aminex HPX-87C column (250 × 4.0 mm) and a refraction index detector (RID).

The total conversion of xylitol (X_{Xy}) to gaseous and liquid products was determined from:

$$X_{Xy} = \frac{F^0_{Xy} - F_{Xy}}{F^0_{Xy}} \tag{4}$$

where F^0_{Xy} and F_{Xy} are the xylitol molar flow at the inlet and the exit of the reactor, respectively. The carbon-based conversion of xylitol to gaseous products was calculated as:

$$X^G_{Xy} = \frac{\sum \alpha_i F_i}{\alpha_{Xy} F^0_{Xy}} \tag{5}$$

where α_i is the number of C atoms in the product i molecule, F_i the molar flow of gaseous product i formed from xylitol, and α_{Xy} the number of C atoms in the xylitol molecule. The C-containing gaseous products formed from xylitol were CO, CO_2 and CH_4, so that X^G_{Xy} became:

$$X^G_{Xy} = \frac{F_{CO} + F_{CH_4} + F_{CO_2}}{5\, F^0_{Xy}} \tag{6}$$

The conversion of xylitol to liquid products, X^L_{Xy}, was calculated as the difference between X_{Xy} and X^G_{Xy}. The yield to H_2 (η_{H_2}, moles of H_2 produced/moles of xylitol fed) was calculated by taking into account the stoichiometric factors of reaction 3:

$$\eta_{H_2} = \frac{F_{H_2}}{F^0_{Xy}} \cdot \frac{1}{11} \tag{7}$$

The selectivity to H_2 in the gas phase is defined as S_{H_2} = molecules H_2 produced/C atoms in gas phase. In our catalytic runs the amount of C_2–C_6 hydrocarbons in the gas phase was lower than 1% in all the cases, which is consistent with results reported in previous work on APR of polyols when no hydrogen is fed to the reactor [3,15], as is the case here. Then, the H_2 selectivity was determined as:

$$S_{H_2} = \frac{F_{H_2}}{F_{CO} + F_{CO_2} + F_{CH_4}} \cdot \frac{1}{RR} \quad (8)$$

where RR, the H_2/CO_2 reforming ratio, is 11/5 and represents the maximum H_2/C molar ratio that can be obtained according to the stoichiometry of reaction 3. The H_2 productivity (Pr, mol H_2/h g_{cat}) is actually the H_2 formation rate and was calculated as

$$Pr = \frac{F_{H_2}}{W_{cat}} . \quad (9)$$

Results and discussion

Catalyst characterization

The acid properties of alumina Ketjen CK300 were determined by TPD of NH_3, IR spectroscopy, and FTIR spectra of adsorbed pyridine. Results are shown in Fig. 2. The asymmetric NH_3 desorption rate curve presented a maximum at about 500 K (Fig. 2A). From deconvolution and integration of the NH_3 TPD curve we determined a value of 19 μmol NH_3/g for the density of surface acid sites, which is consistent with NH_3 TPD values reported in previous work showing that commercial Al_2O_3 CK-300 is a medium-strength acid material [31,32]. Fig. 2B presents the Al_2O_3 IR spectrum obtained in the hydroxyl stretching region after evacuation at 723 K for 2 h. No absorption bands were detected thereby indicating that the hydroxyl group concentration in our support is negligible. On the other hand, the nature of Al_2O_3 surface acid sites was also established from the FTIR spectra of adsorbed pyridine. Fig. 2C shows the spectra obtained after admission of pyridine, adsorption at room temperature, and sequential evacuation at 303 and 373 K. The pyridine absorption bands at around 1540 cm^{-1} and 1450 cm^{-1} arise from pyridine adsorbed on Brønsted and Lewis acid sites, respectively. The IR spectra of Fig. 2C confirm that Al_2O_3 CK300 contains essentially Lewis acid sites.

The X-ray diffractograms of Al_2O_3, Pt(1.50)/Al_2O_3 and Pt(2.77)/Al_2O_3 are given in Fig. 3. The XRD patterns of Pt catalysts exhibited only the alumina crystalline structure of the support. The fact that no crystalline phase of Pt was detected indicates that the Pt crystallite sizes are lower than the detection limit of the XRD unit (about 40 Å) and suggests that the metal was well dispersed on the support.

The Pt loading, surface area (S_{BET}), Pt dispersion (D_{Pt}), mean Pt particle size ($\bar{d}_{Pt}$) and Pt surface concentration of Pt/Al_2O_3 catalysts are presented in Table 1. The BET surface area of Al_2O_3 CK300 (220 m^2/g) did not change significantly after the metal impregnation and the consecutive oxidation/reduction steps used for obtaining Pt/Al_2O_3 catalysts. The Pt dispersion decreased slightly with the metal loading, from 67% on Pt(0.30)/Al_2O_3 to 54% on Pt(2.77)/Al_2O_3, reflecting the $\bar{d}_{Pt}$ increase from 1.3 nm to 1.6 nm, respectively.

Samples Pt(1.50)/Al_2O_3 and Pt(2.77)/Al_2O_3 were also observed by transmission electron microscopy. Fig. 4A shows a TEM image and the size distribution histogram of fresh

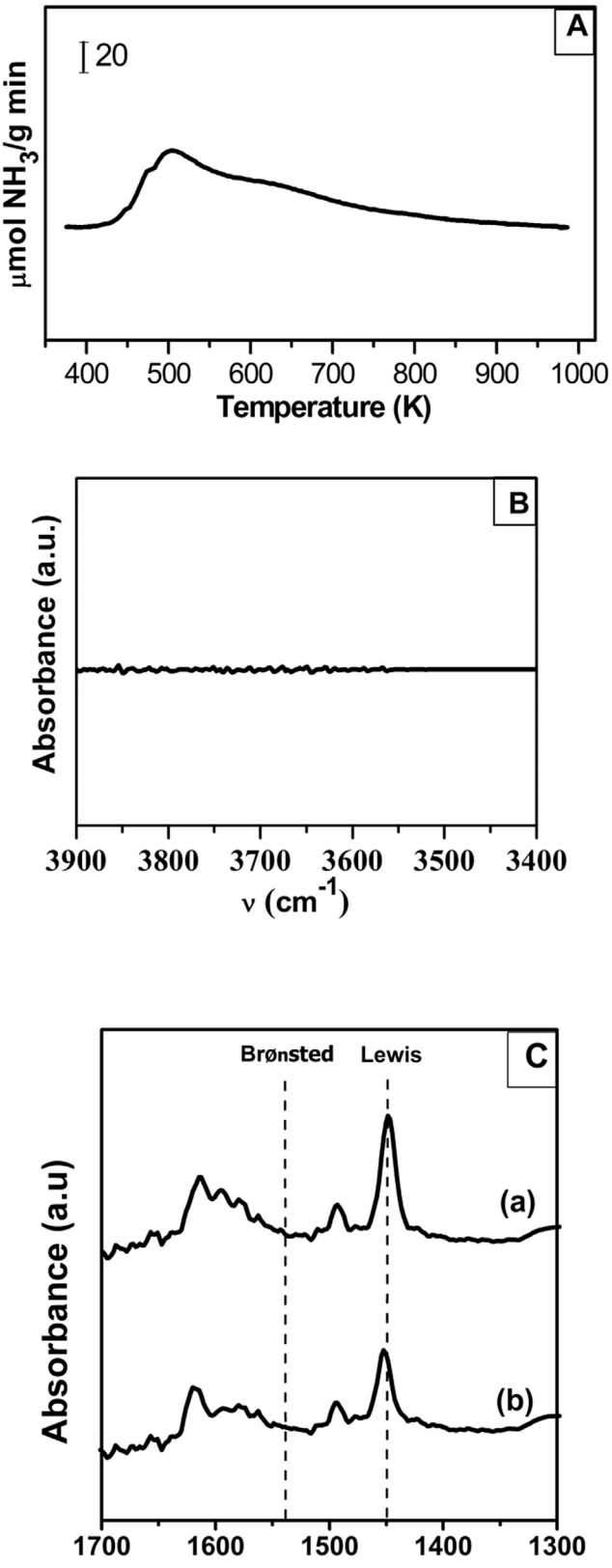

Fig. 2 – Surface acidity of Al_2O_3 support. (A): TPD of NH_3; (B): IR spectrum in the hydroxyls region; (C): IR spectra of pyridine adsorbed at 298 K and evacuated at 303 K (a) and 373 K (b).

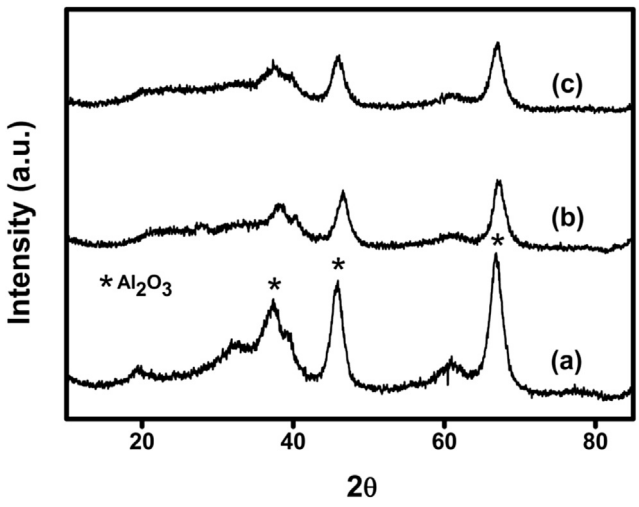

Fig. 3 – Sample characterization by X-ray diffraction: XRD diffractograms of Al_2O_3 (a), Pt(1.50)/Al_2O_3 (b) and Pt(2.77)/Al_2O_3 (c).

Pt(2.77)/Al_2O_3 sample. The d_{VA} values determined by TEM for Pt(1.50)/Al_2O_3 and Pt(2.77)/Al_2O_3 were consistent with the corresponding $\overline{d}_{Pt}$ values obtained by H_2 chemisorption (Table 1).

Catalytic results

Fig. 5 shows xylitol conversions (X_{Xy}, X^G_{Xy} , X^L_{Xy}) and H_2 selectivity (S_{H_2}) obtained at 498 K on Pt(1.50)/Al_2O_3 and typically illustrates the time-on-stream behavior observed for our Pt/Al_2O_3 catalysts during the APR reaction. In all the cases, the start-up of the reaction required about 150 min to obtain stationary values of xylitol conversions and H_2 selectivity. The catalyst activity and selectivity remained constant then up to the end of the 12-h catalytic run. Although previous work [33,34] has shown that in the conditions of APR of polyols on Pt/Al_2O_3, alumina is slowly converted to boehmite, which may deactivate the catalyst, we did not observe any activity decay in our short-term catalytic runs. The results reported in this work were all obtained from the stationary region of catalytic runs, typically represented in Fig. 5.

Table 1 – Physicochemical properties of Pt/Al_2O_3 catalysts.

Catalyst	Pt loading (%wt)	S_{BET} (m^2/g)	D_{Pt} [a] (%)	$\overline{d}_{Pt}$ [a] (nm)	Surface Pt concentration (μmol Pt/g_{cat})	d_{VA} [b] (nm)
Pt(0.30)/Al_2O_3	0.30	217	67	1.3	10.3	–
Pt(0.57)/Al_2O_3	0.57	223	63	1.4	18.4	–
Pt(1.50)/Al_2O_3	1.50	206	56	1.5	43.1	1.9
Pt(2.77)/Al_2O_3	2.77	209	54	1.6	76.7	2.0

[a] Determined by H_2 chemisorption.
[b] Determined by TEM.

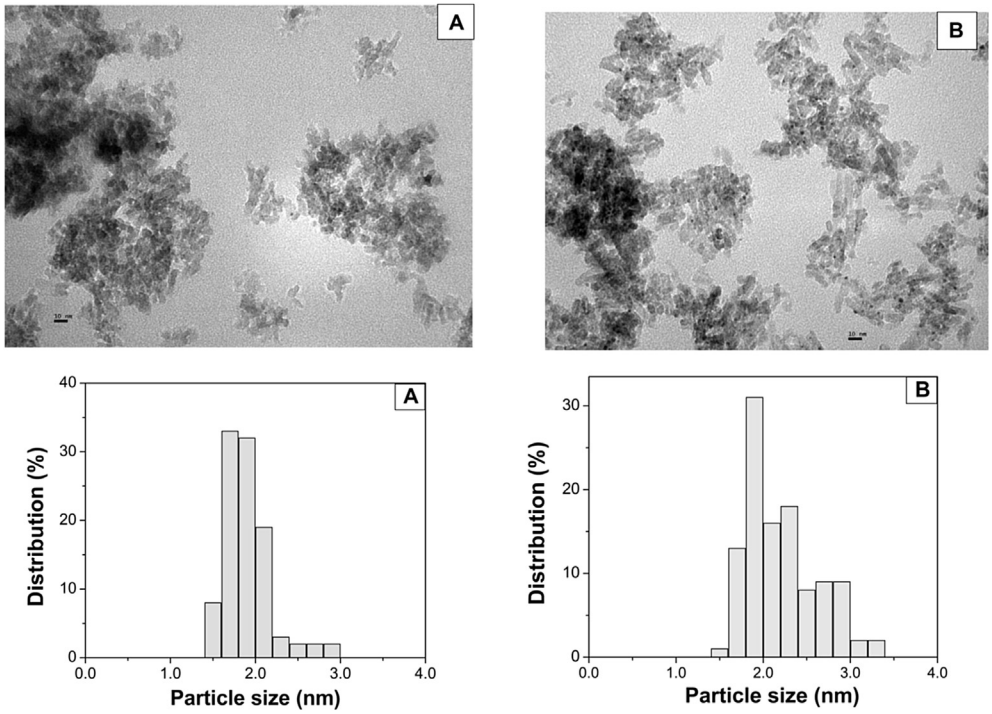

Fig. 4 – TEM images and size distribution histograms of fresh (A) and used (B) Pt(2.77)/Al_2O_3 catalyst.

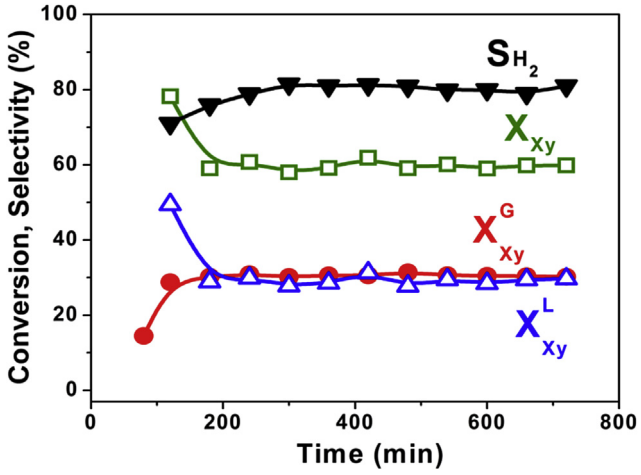

Fig. 5 – Xylitol conversions (X_{Xy}, X^G_{Xy}, X^L_{Xy}) and H_2 selectivity (S_{H_2}) as a function of time [Catalyst: Pt(1.50)/Al_2O_3, T = 498 K, P = 29.3 bar; WHSV = 1.2 h^{-1}, Feed: xylitol(1.0%)/water].

In Fig. 6 we plotted the evolution of xylitol conversions and H_2 selectivity and yield as a function of space velocity obtained on Pt(1.50)/Al_2O_3. As expected, X_{Xy} and X^G_{Xy} diminished with WHSV as well as η_{H_2}. In contrast, S_{H_2} continuously increased when varying WHSV from 0.4 h^{-1} to 2.4 h^{-1}. The fact that the H_2 selectivity increases with an increase in space velocity has been previously observed for the APR of polyols [15,35] and was attributed to larger H_2 consumption in hydrogenolysis/hydrogenation side-reactions at higher reactant conversion levels (i.e. at lower space velocities). A similar qualitative effect of the space velocity on catalyst activity and selectivity showed in Fig. 6 for Pt(1.50)/Al_2O_3 was observed on the other Pt catalysts used in this work.

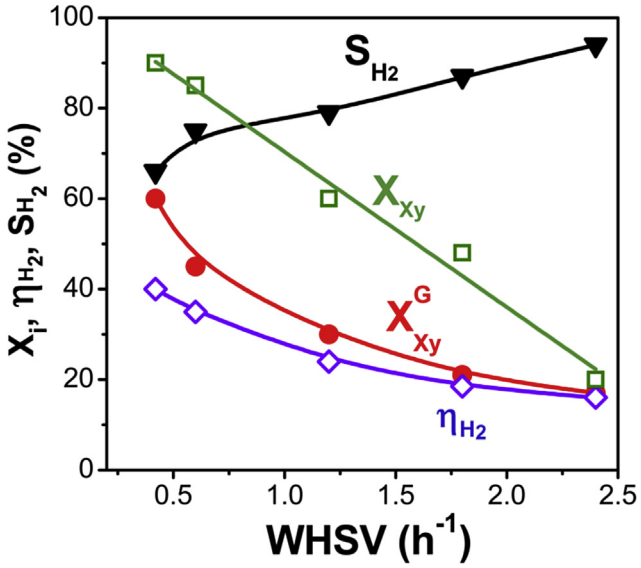

Fig. 6 – APR of xylitol: Effect of space velocity [Catalyst: Pt(1.50)/Al_2O_3, T = 498 K; P = 29.3 bar; W_{cat} = 0.1 g; Feed: xylitol(1.0%)/water].

The effect of Pt_s (surface Pt concentration, Table 1) on catalyst activity at WHSV = 1.2 h^{-1} is presented in Fig. 7. The total conversion of xylitol, X_{Xy}, increased with Pt_s, reflecting mainly the increase of X^G_{Xy}. The xylitol conversion to liquid products, X^L_{Xy}, did not change significantly when Pt_s was varied between 10.3 and 76.7 μmol Pt/g_{cat}. It seems then that the gaseous/liquid products ratio depends on the amount of surface Pt concentration on the sample. This is an important result considering that the selective conversion of xylitol to gaseous products is required to obtain high H_2 productivities. In order to obtain more insight on the effect of Pt_s on catalyst activity, we plotted in Fig. 8 the evolution of X^G_{Xy} and X^L_{Xy} as a function of X_{Xy} on all the catalysts. X^L_{Xy} increased almost linearly with X_{Xy} on Pt/Al_2O_3 catalysts, excepting on Pt(2.77)/Al_2O_3. In the X_{Xy} < 25% region, the X^G_{Xy}/X^L_{Xy} ratio was higher than one in all the cases. For X_{Xy} values higher than about 25%, the X^G_{Xy}/X^L_{Xy} ratio was lower than one on Pt(0.30)/Al_2O_3 and Pt(0.57)/Al_2O, but higher than one on Pt(1.50)/Al_2O_3 and Pt(2.77)/Al_2O. Thus, results in Fig. 8 confirm that the ratio of gaseous to liquid products obtained from xylitol conversion on Pt/Al_2O_3 catalysts depends on Pt content.

The effect of surface Pt concentration of Pt/Al_2O_3 catalysts on H_2 selectivity is presented in Fig. 9 at three X_{Xy} levels: 15%, 50% and 85%. S_{H_2} continuously increased with Pt_s, irrespective of the X_{Xy} value, thereby showing that the H_2 concentration in the gas phase is improved by the amount of accessible platinum. On the other hand, Fig. 10 also shows that at a given Pt_s value, S_{H_2} increases when xylitol conversion decreases, which is consistent with the results presented in Fig. 6 for Pt(1.50)/Al_2O_3. More information on the effect of Pt loading on product distribution in the gas phase is presented in Table 2, which shows the results obtained at two space velocities (0.6 h^{-1} and 2.4 h^{-1}). In agreement with data in Fig. 9, Table 2 shows that for a given WHSV value, the H_2 concentration in the gas phase increases with the Pt loading. At WHSV = 2.4 h^{-1}, the H_2 concentration increased from 64.1% (0.30% Pt) to 67.7% (2.77% Pt). This later value is close to the stoichiometric production of H_2 predicted by reaction 3 (68.75%).

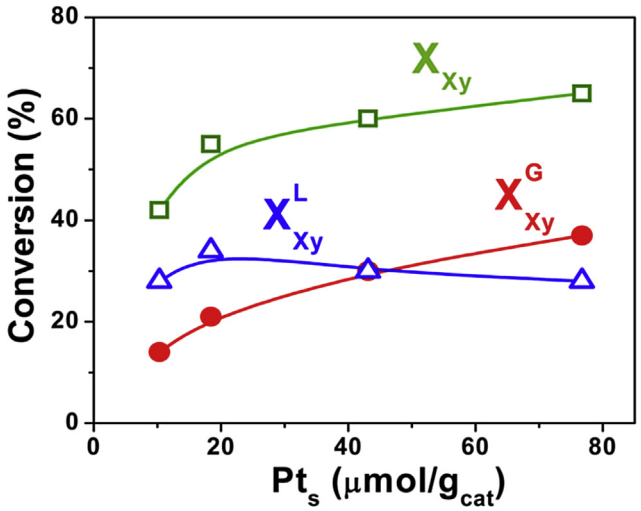

Fig. 7 – Effect of surface Pt concentration on catalyst activity [T = 498 K, P = 29.3 bar; WHSV = 1.2 h^{-1}, Feed: xylitol(1.0%)/water].

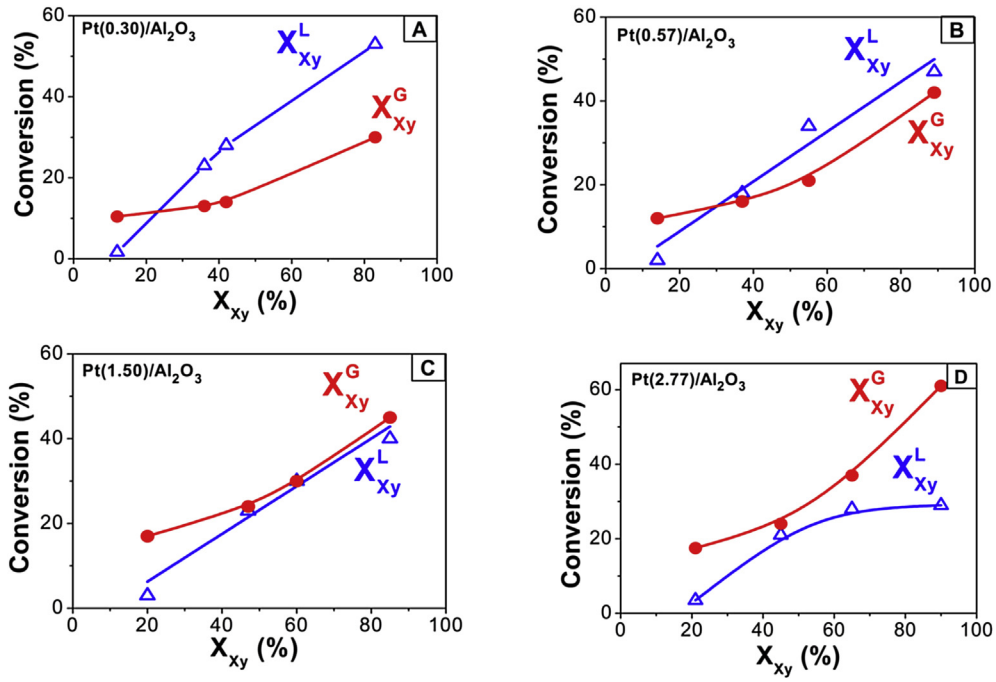

Fig. 8 – Effect of metal loading on xylitol conversion to gas and liquid products [T = 498 K; P = 29.3 bar; W_{cat} = 0.1 g; Feed: xylitol(1%)/water].

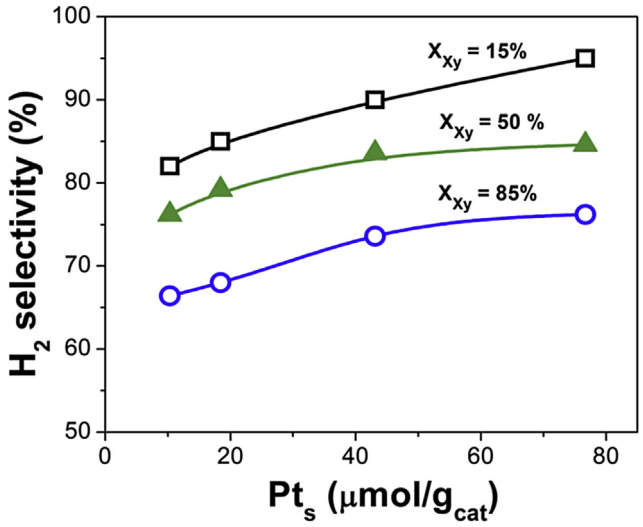

Fig. 9 – H_2 selectivity as a function of surface Pt concentration at constant xylitol conversions [T = 498 K; P = 29.3 bar; Feed: xylitol(1%)/water].

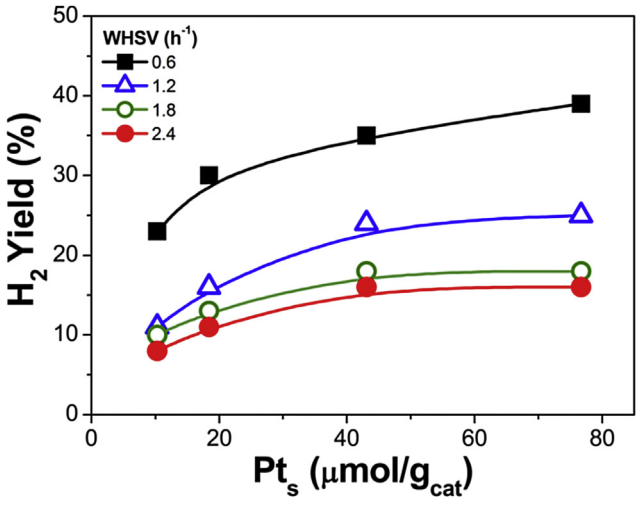

Fig. 10 – H_2 yield as a function of surface Pt concentration. Reactions conditions as in Fig. 8.

In Fig. 10 we plotted the H_2 yield as a function of Pt_s for different space velocities. At a given Pt_s value, η_{H_2} increased with contact time (i.e. when WHSV was diminished), reflecting essentially the simultaneous increase of xylitol conversion. At a given space velocity, η_{H_2} increased continuously with Pt_s, probably because X_{Xy} also increased with Pt_s, as shown in Fig. 7. The maximum H_2 yield (39%) was then obtained on Pt(2.77)/Al_2O_3 at WHSV = 0.6 h^{-1}. Kirilin et al. [15] investigated the production of H_2 by APR of xylitol on Pt(5%)/Al_2O_3 at 498 K, 29.3 bar and 10 wt.% xylitol in the feed, using space velocities between 1.2 and 3.9 h^{-1}; they obtained a maximum H_2 yield of 32% at WHSV = 1.8 h^{-1}. Kim et al. [19] studied the APR of 10% xylitol at WHSV = 2 h^{-1} on 7% Pt/carbon using different pressures (28–45 bar) and temperatures (493–523 K); they reported a maximum η_{H_2} value of 35.4% at 523 K and 45 bar.

The key parameter for evaluating the APR process economy is the H_2 productivity, Pr (mol H_2/g_{cat} h), that is expressed as:

$$Pr = \frac{F_{H_2}}{W_{cat}} = \eta_{H_2}\ WHSV\ \frac{11}{M_{Xy}} \qquad (10)$$

Table 2 – APR of xylitol: Product distribution in the gas phase.

Catalyst	WHSV = 0.6 h^{-1}							WHSV = 2.4 h^{-1}						
	Xylitol conversions			Gas phase composition				Xylitol conversions			Gas phase composition			
	X_{Xy}	X^G_{Xy}	X^L_{Xy}	H_2	CO	CH_4	CO_2	X_{Xy}	X^G_{Xy}	X^L_{Xy}	H_2	CO	CH_4	CO_2
$Pt(0.30)/Al_2O_3$	83	30	53	59.3	0.6	3.6	36.5	12	11	1	64.1	0.10	4.0	31.8
$Pt(0.57)/Al_2O_3$	85	42	47	60.0	0.3	4.1	35.6	14	12	2	65.7	0.8	4.0	29.4
$Pt(1.50)/Al_2O_3$	89	45	40	61.6	0.5	3.0	34.9	20	17	3	66.4	0.3	3.8	29.5
$Pt(2.77)/Al_2O_3$	90	61	29	62.5	0.07	3.4	34.3	21	17	4	67.7	0.08	3.1	29.5

Results obtained at the end of catalytic runs. All the values are in %.
[T = 498 K; P = 29.3 bar; W_{cat} = 0.1 g; Feed: Xylitol(1.0%)/water].

where M_{Xy} is the molecular weight of xylitol. According to Eq. (4), the H_2 productivity increases with WHSV but, as shown in Fig. 10, η_{H_2} diminishes when WHSV increased. Consequently, Eq. (10) implicitly predicts that Pr plots may go through a maximum when representing as a function of WHSV. Actually, previous work on APR of polyols have reported the existence of H_2 productivities maxima when the space velocity is varied [11,15]. Here, we plotted in Fig. 11 the H_2 productivity as a function of Pt_s for different space velocities. On the four Pt catalysts, Pr increased initially with Pt_s but then reached a plateau at a surface Pt concentration of about 40 μmol/g_{cat} ($Pt(1.5)/Al_2O_3$ catalyst). Fig. 11 also shows that at a given Pt_s value, Pr increased in all the cases with WHSV; i.e., we did not observe any Pr maximum within the range of space velocities investigated. The maximum H_2 productivity (28 mmol H_2/g_{cat} h) was obtained then on $Pt(1.5)/Al_2O_3$ and $Pt(2.77)/Al_2O_3$ catalysts at WHSV = 2.4 h^{-1}. Finally, it is worth noting that Fig. 11 shows that at a given WHSV the H_2 productivity did not increase significantly as the Pt surface concentration was increased from 40 to 80 μmol/g. This result suggests that no significant gain in H_2 productivity should be expected using Pt_s values higher than about 40 μmol/g that in our case corresponded to a Pt/Al_2O_3 catalysts containing 1.5% Pt.

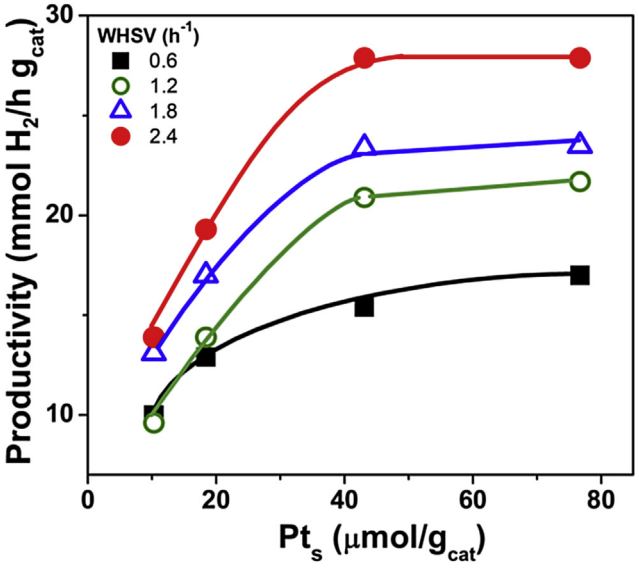

Fig. 11 – H_2 productivity as a function of surface Pt concentration. Reactions conditions as in Fig. 8.

A literature survey shows that at WHSV = 2.4 h^{-1} Kirilin et al. [15] obtained H_2 productivities of about 40 mmol H_2/g_{cat} h for APR of xylitol on $Pt(5\%)/Al_2O_3$ at 498 K, 29.3 bar and 10 wt.% xylitol in the feed. At WHSV = 2 h^{-1}, 493 K, 28 atm, and 10% xylitol, Kim et al. [19] yielded 18 mmol H_2/g_{cat} h^{-1} on Pt(7%)/carbon. When Pt was supported on supports more acid than alumina such as TiO_2, carbon or zeolites, the H_2 productivity by APR of xylitol was significantly lower than the maximum Pr value reported in this work [16,17]. Bimetallic $Pt–Re/Al_2O_3$ also produces less H_2 than Pt/Al_2O_3 [17].

We also studied the effect of xylitol concentration on H_2 productivity. Catalytic runs were performed on $Pt(2.77)/Al_2O_3$ at different space velocities using xylitol/water feeds containing 1.0, 3.3, 5.0 and 10% xylitol; results are presented in Table 3. At WHSV = 1.2 h^{-1} (rows 1 to 3 in Table 3), the total conversion of xylitol increased with xylitol concentration, from 65% (1.0% xylitol) to 95% (5.0% xylitol), due mainly to the corresponding increase of X^L_{Xy} from 28% to 50%. In contrast, S_{H_2} and the H_2 concentration in the gas phase significantly diminished with increasing xylitol concentration in the feed. The H_2 productivity slightly decreased when xylitol

Table 3 – Effect of xylitol concentration on catalyst activity, selectivity, yield and productivity.

Xylitol concentration (% wt)	WHSV (h^{-1})	X_{Xy} (%)	X^G_{Xy} (%)	X^L_{Xy} (%)	S_{H_2} (%)	η_{H_2} (%)	Productivity (mmol H_2/h g_{cat})	Gas phase composition (% molar)			
								H_2	CO	CH_4	CO_2
1.0	1.2	65	37	28	68	25	21.7	60.6	0.07	3.0	36.3
3.3	1.2	90	45	45	50	23	21.0	50.3	0.5	3.6	45.5
5.0	1.2	95	45	50	45	20	19.2	49.6	0.8	4.3	45.0
5.0	6.0	22	8	14	88	7	30.7	66.0	0.2	2.7	31.0
10.0	12.0	4.2	4	0.2	98	4	35.0	68.0	0.2	2.6	30.0

[Catalyst: $Pt(2.77)/Al_2O_3$; T = 498 K; P = 29.3 bar].

Table 4 – APR of xylitol: characterization of the metal fraction before and after reaction [T = 498 K; P = 29.3 bar; WHSV = 1.2 h^{-1}; Feed: Xylitol(1.0%)/water].

Catalyst	Reaction length (h)	Pt dispersion (%)[a]		d_{VA} (nm)[b]	
		Fresh	Used	Fresh	Used
$Pt(0.30)/Al_2O_3$	12	67	28	–	–
$Pt(0.57)/Al_2O_3$	5	63	35	–	–
$Pt(1.50)/Al_2O_3$	12	56	15	1.9	2.2
$Pt(2.77)/Al_2O_3$	5	54	26	2.0	2.4

[a] Determined by H_2 chemisorption.
[b] Determined by TEM.

concentration was increased from 1.0% (Pr = 21.7 mmol H_2/h g_{cat}) to 5.0% (Pr = 19.2 mmol H_2/h g_{cat}) at WHSV = 1.2 h^{-1}. The effect of xylitol concentration on H_2 productivity was also investigated at different space velocities. Specifically, Table 3 shows the results obtained at space velocities of 1.2 h^{-1} (first row), 6.0 h^{-1} (fourth row) and 12.0 h^{-1} (fifth row). It is observed that S_{H_2} and Pr increased when xylitol concentration and WHSV were increased. Using 10% xylitol at WHSV = 12.0 h^{-1}, the H_2 selectivity increased to 98% and the H_2 productivity to 35.0 mmol H_2/h g_{cat}.

Finally, we characterized the metallic fraction of the catalysts before and after reaction in order to obtain insight on the platinum sintering on stream. Specifically, at the end of catalytic runs of 5–12 h length, we purged the reactor with nitrogen and then the catalysts were contacted with flowing air at 573 K for 3 h for eliminating adsorbed products and coke precursors. Then, we determined the platinum dispersion by H_2 chemisorption. Used $Pt(1.50)/Al_2O_3$ and $Pt(2.77)/Al_2O_3$ samples were also characterized by TEM. Results are presented in Table 4 and Fig. 4. In all the cases, a severe Pt sintering was observed. For a given reaction length, the Pt dispersion drop increased with Pt loading. For example, after a 12-h reaction run, D_{Pt} on $Pt(0.30)/Al_2O_3$ and $Pt(1.50)/Al_2O_3$ diminished 58% and 73%, respectively; similarly, in catalytic tests of 5-h length, D_{Pt} on $Pt(0.57)/Al_2O_3$ and $Pt(2.77)/Al_2O_3$ decreased 45% and 52%, respectively. The d_{av} values (Table 4) and the size distribution histograms (Fig. 4) determined by TEM for $Pt(1.50)/Al_2O_3$ and $Pt(1.50)/Al_2O_3$ confirmed that the Pt crystallites sintered during the APR of xylitol. Results in Table 4 are in agreement with previous work that reported the on-stream Pt particle sintering under APR reaction conditions [29,36]. Platinum sintering has been associated to the presence of significant amounts of water during the APR reaction and to degradation of the support. Nevertheless, it is worth noting here that during the standard catalytic tests of 12 h length we did not observe any significant activity decay after stationary conditions were reached, on all the Pt/Al_2O_3 catalysts investigated (Fig. 5 shows as an example the evolution of xylitol conversion as a function of time obtained on $Pt(1.50)/Al_2O_3$). An additional catalytic run of 36 h length carried out on $Pt(1.50)/Al_2O_3$ confirmed that the catalyst activity and selectivity remained constant on stream. Because Pt sintering is an important cause for loss of catalyst activity, we infer that the loss of Pt surface area observed in Table 4 would occur essentially during the catalyst work-up, at the beginning of the catalytic run (Fig. 5). Clearly, more research and insight are needed to establish the on-stream Pt sintering kinetics during the APR of polyols on Pt/Al_2O_3 catalysts.

Conclusions

The production of H_2 by aqueous-phase reforming of 1% xylitol at 498 K and 29.3 bar on Pt/Al_2O_3 catalysts depends on the space velocity and the surface Pt concentration (Pt_s). In this work, Pt_s was varied between 10.3 μmol Pt/g_{cat} ($Pt(0.30)/Al_2O_3$) and 76.7 μmol Pt/g_{cat} ($Pt(2.77)/Al_2O_3$). At a given space velocity, the gaseous/liquid products ratio increases with Pt_s. For xylitol conversions lower than about 25% (i.e. at high WHSV values) the X^G_{Xy}/X_{Xy} ratio was close to 0.9 on all the catalysts. At a given xylitol conversion, the H_2 selectivity increases with Pt_s, irrespective of the X_{Xy} value.

The H_2 yield increased with contact time and Pt_s, which essentially reflects that xylitol conversion raises when both parameters are increased. Thus, the maximum H_2 yield (39%) was obtained on the catalyst containing the highest Pt loading ($Pt(2.77)/Al_2O_3$) at the lower space velocity (WHSV = 0.6 h^{-1}). The H_2 productivity increases with both Pt_s and WHSV. At a given WHSV, the H_2 productivity increases continuously with Pt_s but reaches a plateau at about 40 μmol Pt/g that in our case corresponded to a Pt/Al_2O_3 catalysts containing 1.5% Pt. The production of H_2 also depends on the xylitol concentration in the feed. At a constant WHSV value, the total conversion of xylitol increases with xylitol concentration, mainly because of the xylitol conversion increase to liquid products; in contrast, the H_2 selectivity and productivity decrease with increasing xylitol concentration.

Acknowledgements

Authors thank the Universidad Nacional del Litoral (UNL), Consejo Nacional de Investigaciones Científicas y Técnicas (CONICET), and Agencia Nacional de Promoción Científica y Tecnológica (ANPCyT), Argentina, for the financial support of this work.

REFERENCES

[1] Davda RR, Shabaker JW, Huber GW, Cortright RD, Dumesic JA. A review of catalytic issues and process conditions for renewable hydrogen and alkanes by aqueous-phase reforming of oxygenated hydrocarbons over supported metal catalysts. Appl Catal B Environ 2005;56:171–86.
[2] Balat H, Kirtay E. Hydrogen from biomass-present scenario and future prospects. Int J Hydrogen Energy 2010;35:7416–26.
[3] Cortright RD, Davda RR, Dumesic JA. Hydrogen from catalytic reforming of biomass-derived hydrocarbons in liquid water. Nature 2002;418:964–7.
[4] Huber GW, Shabaker JW, Evans ST, Dumesic JA. Aqueous-phase reforming of ethylene glycol over supported Pt and Pd bimetallic catalysts. Appl Catal B Environ 2006;62:226–35.
[5] Shabaker JW, Huber GW, Davda RR, Cortright RD, Dumesic JA. Aqueous-phase reforming of ethylene glycol over supported platinum catalysts. Catal Lett 2003;88:1–8.

[6] Lehnert K, Claus P. Influence of Pt particle size and support type on the aqueous-phase reforming of glycerol. Catal Commun 2008;9:2543–6.
[7] Wawrzetz A, Peng B, Hrabar A, Jentys A, Lemonidou AA, Lercher JA. Towards understanding the bifunctional hydrodeoxygenation and aqueous phase reforming of glycerol. J Catal 2010;269:411–20.
[8] Kim HD, Kim TW, Park HJ, Jeong KE, Chae HJ, Jeong SY, et al. Hydrogen production through the aqueous-phase reforming of ethylene glycol over supported Pt-based bimetallic catalysts. Int J Hydrogen Energy 2012;37:8310.
[9] Tanksale A, Wong Y, Beltramini JN, Lu GQ. Hydrogen generation from liquid phase catalytic reforming of sugar solutions using metal-supported catalysts. Int J Hydrogen Energy 2007;32:717–24.
[10] Wen G, Xu Y, Xu Z, Tian Z. Characterization and catalytic properties of the Ni/Al_2O_3 catalysts for aqueous-phase reforming of glucose. Catal Lett 2009;129:250–7.
[11] Tanksale A, Beltramini JN, Dumesic JA, Lu GQ. Effect of Pt and Pd promoter on Ni supported catalysts-A TPR/TPO/TPD and microcalorimetry study. J Catal 2008;258:366–77.
[12] Kirilin AV, Tokarev AV, Murzina EV, Kustov LM, Mikkola JP, Murzin DYu. Reaction products and transformations of intermediates in the aqueous-phase reforming of sorbitol. ChemSusChem 2010;3:708–18.
[13] Tokarev AV, Kirilin AV, Murzina EV, Eranen K, Kustov LM, Murzin DYu, et al. The role of bio-ethanol in aqueous phase reforming to sustainable hydrogen. Int J Hydrogen Energy 2010;35:12642–9.
[14] Kirilin AV, Wärna J, Tokarev AV, Murzin DYu. Kinetic modeling of sorbitol aqueous-phase reforming over Pt/Al_2O_3. Ind Eng Chem Res 2014;53:4580–8.
[15] Neira D'Angelo MF, Schouten JC, van der Schaaf J, Nijhuis TA. Aqueous phase reforming in a microchannel reactor: the effect of mass transfer on hydrogen selectivity. Catal Sci Technol 2013;3:2834–42.
[16] Kirilin AV, Tokarev AV, Kustov LM, Salmi T, Mikkola JP, Murzin DYu. Aqueous phase reforming of xylitol and sorbitol: comparison and influence of substrate structure. Appl Catal A General 2012;435–436:172–80.
[17] Jiang T, Wang T, Ma L, Li Y, Zhang Q, Zhang X. Investigation on the xylitol aqueous-phase reforming performance for pentane production over Pt/HZSM-5 and Ni/HZSM-5 catalysts. Appl Energy 2012;90:51–7.
[18] Kirilin AV, Tokarev AV, Manyar H, Hardacre C, Salmi T, Mikkola JP, et al. Aqueous phase reforming of xylitol over Pt-Re bimetallic catalyst: effect of the Re addition. Catal Today 2014;223:97–107.
[19] Kirilin AV, Hasse B, Tokarev AV, Kustov LM, Baeva GN, Bragin GO, et al. Aqueous-phase reforming of xylitol over Pt/C and Pt/TiC-CDC catalysts: catalyst characterization and catalytic performance. Catal Sci Technol 2014;4:387–401.
[20] Kim TW, Kim MC, Yang YC, Kim YR, Jeong SY, Kim CU. Hydrogen production via the aqueous phase reforming of polyols over CMK-9 mesoporous carbon supported platinum catalysts. Int J Hydrogen Energy 2015;40:15236–43.
[21] Simonetti DA, Dumesic JA. Catalytic production of liquid fuels from biomass-derived oxygenated hydrocarbons: catalytic coupling at multiple length scales. Catal Rev 2009;51:441–84.
[22] Huber GW, Dumesic JA. An overview of aqueous-phase catalytic processes for production of hydrogen and alkanes in a biorefinery. Catal Today 2006;111:119–32.
[23] Fengel D, Wegener G, Heizmann A, Przyklenk M. Cell Chem Technol 1978;12:31–7.
[24] Willför S, Sundberg A, Pranovich A, Holmbom B. Polysaccharides in some industrially important hardwood species. Wood Sci Technol 2005;39:601–17.
[25] Rafiqul ISM, Mimi Sakinah AM. Design of process parameters for the production of xylose from wood sawdust. Chem Eng Res Des 2012;90:1307–12.
[26] Davda RR, Shabaker JW, Huber GW, Cortright RD, Dumesic JA. Aqueous-phase reforming of ethylene glycol on silica-supported metal catalysts. Appl Catal B Environ 2003;43:13–26.
[27] Huber GW, Cortright RD, Dumesic JA. Renewable alkanes by aqueous-phase reforming of biomass-derived oxygenates. Angew Chem Int Ed 2004;43:1549–51.
[28] Kim TW, Kim HD, Jeong KE, Chae HJ, Jeong SY, Lee CH, Kim CU. Catalytic production of hydrogen through aqueous-phase reforming over platinum/ordered mesoporous carbon catalysts. Green Chem 2011;13:1718–28.
[29] Yamaguchi W, Tai Y. Size-dependent catalytic activity of platinum nanoparticles for aqueous-phase reforming of glycerol. Chem Lett 2014;43:313–5.
[30] Garetto TF, Apesteguía CR. Oxidative catalytic removal of hydrocarbons over Pt/Al_2O_3 catalysts. Catal Today 2000;62:189–99.
[31] Garetto TF, Rincón E, Apesteguía CR. The origin of the enhanced activity of Pt/zeolites for combustion of C_2-C_4 alkanes. Appl Catal B Environ 2007;73:65–72.
[32] Bertero NM, Trasarti AF, Apesteguía CR, Marchi AJ. Liquid-phase dehydration of 1-phenylethanol on acid solids: influence of catalyst acidity and pore structure. Appl Catal A General 2013;458:28–38.
[33] Ravenelle RM, Copeland JR, Kim WG, Crittenden JC, Sievers C. Structural changes of γ-Al_2O_3-supported catalysts in hot liquid water. ACS Catal 2011;1:552–61.
[34] Ciftci A, Peng B, Jentys A, Lercher JA, Hensen EJM. Support effects in the aqueous phase reforming of glycerol over supported platinum catalysts. Appl Catal A General 2012;431–432:113–9.
[35] Li N, Huber GW. Aqueous-phase hydrodeoxygenation of sorbitol with Pt/SiO_2-Al_2O_3: identification of reaction intermediates. J Catal 2010;270:48–59.
[36] Maris EP, Davis RJ. Hydrogenolysis of glycerol over carbon-supported Ru and Pt catalysts. J Catal 2007;249:328–37.